Archive of Applied Mechanics 70 (2000) 47–64 © Springer-Verlag 2000

Phenomenological modeling and numerical simulation of the environmental degradation of multiphase engineering materials

T. I. Zohdi, P. Wriggers

Summary In this paper a coupled thermodynamical/chemical/mechanical model is developed to simulate the time dependent degradation of heterogeneous solid materials subjected to corrosive environments. The model, which is based on a description of the microscale, employs the first law of thermodynamics, a mass balance of a diffusing corrosive species, and a balance of momentum. The presence of the corrosive species is phenomenologically modeled as irreversibly reducing the material stiffness, dependent on the amount and time present. Numerical experiments are given to illustrate some characteristics of the model.

Key words Multiphase materials, micromechanics, environmental degradation

1 Introduction

In the last two decades, composite materials developed and processed through a variety of methods have become widely used in engineering designs. However, in many industrial applications, the theoretically designed composite material properties are lost due to contact with corrosive environments. In this paper, we refer to corrosion as an undesired degradation of a material through chemical interaction. It is critical to emphasize that the phenomena of chemical degradation is material-dependent, and that no unified theory exists, nor is one proposed. However, there is some phenomenological similarities, namely, the reduction of the material stiffness at a macroscopic point, depending on the amount of the corrosive present and its time duration. In many cases, the degradation of the mechanical properties of structural materials can be traced to the absorption of excessive amounts of corrosive substance, for example hydrogen, in combination with residual or applied tensile stresses. In particular, metallic solids with heterogeneous microstructure are extremely vulnerable to such degradation, due to their amplified and highly oscillatory internal fields. Therefore, for a composite material to be properly evaluated, its response in the environment that it is planned to be used in must be determined. In total, it is estimated that roughly between US$ 8 to 15 billion are spent yearly to combat corrosion throughout Europe.

With regards to the phenomenon of corrosion, a structural analyst's primary interest is related to the time-dependent changes in the macroscopic response of the material, in particular, its overall stiffness, due to the penetration and continued presence of the corrosive species. The usual procedure in engineering is to describe the undamaged macroscopic aggregate response or "effective" constitutive relation of a micro-heterogeneous material, by a relation between volumetrically averaged stress and strain in a statistically representative volume element (RVE). Typically one determines $\mathbb{E}^*$, where

$$\langle \boldsymbol{\sigma} \rangle_{\Omega} = \mathbb{E}^* : \langle \boldsymbol{\epsilon} \rangle_{\Omega} \ ,$$

with

$$\langle \cdot \rangle_{\Omega} \stackrel{\text{def}}{=} \frac{1}{|\Omega|} \int_{\Omega} \cdot \, \mathrm{d}x \ .$$

In this definition, $\boldsymbol{\sigma}$ and $\boldsymbol{\epsilon}$ are the stress and strain fields within the domain Ω, $\mathbb{E}$ is a spatially variable symmetric, positive definite fourth rank linear elasticity tensor, and

Received 30 March 1999; accepted for publication 30 April 1999

T. I. Zohdi, P. Wriggers
Institut für Baumechanik und Numerische Mechanik
Appelstrasse 9A, D-30167 Hannover, Germany

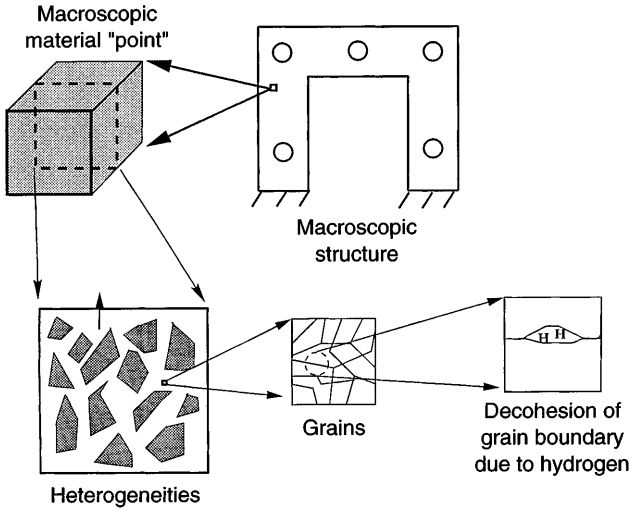

Fig. 1. Multiple scales: damage in the heterogeneous sample is caused by, decohesion on the granular level due to hydrogen

$$\boldsymbol{\epsilon} \stackrel{\text{def}}{=} \frac{\nabla \mathbf{u} + (\nabla \mathbf{u})^{\mathrm{T}}}{2}$$

is the infinitesimal strain, where $\mathbf{u}$ is the displacement field. Pointwise, we have

$$\boldsymbol{\sigma} = \mathbb{E} : \boldsymbol{\epsilon} \ ,$$

where all quantities are functions of time and space unless explicitly stated otherwise. The Tensor $\mathbb{E}^*$, which represents the macroscopic response, has constant components. For the relation between the averages to provide meaningful information, the sample size may have to be quite large relative to the intrinsic length scales of the microstructure, i.e. it must be statistically representative. Ideally, one would like to estimate computationally the loss in a theoretically designed $\mathbb{E}^*$ as a function of the environment and time, by numerical simulation of the degradation of statistically representative samples of material. In order to reduce laboratory expense, the end goal would be to predict the life expectancy of structures exposed to hazardous environments with help from computational simulations.

1.1
Objective

Our objective in this paper is to develop a phenomenological model that can help study the macroscopic response of a representative sample of a heterogeneous material undergoing chemical attack from a corrosive environment. The exact underlying degradation mechanism is essentially irrelevant in this work. The approach is to describe the time-dependent degradation of the macroscopic aggregate's mechanical properties by a stress-assisted diffusion model, where the material strength on the microscopic scale is irreversibly damaged by the growing and/or continued presence of a corrosive substance. The model, which is based on a description of the microscale, employs the first law of thermodynamics, a mass balance of a diffusing corrosive species and a balance of momentum. The outline of the paper is as follows: the governing equations for the coupled fields are derived in Sec. 2, coupling between the fields is discussed in Sec. 3, and approximations are made to simplify the analysis in Sec. 4. In Sec. 5, an intergranular decohesion analysis is performed to obtain phenomenological corrosion parameters for the continuum scale. In Sec. 6, numerical experiments are carried out on a large sample of composite material, and concluding remarks are given. While we do not restrict our attention to any specific type of chemical damage, hydrogen damage due to its widespread industrial occurrence, will be used later in the paper as a representative example.

2
Multifield coupling and phenomenological corrosion

We consider a structure which occupies an open-bounded domain in $\Omega \in \mathbb{R}^3$. Its boundary is denoted $\partial\Omega$. The body is in equilibrium under the action of body forces $\mathbf{b}$ and surface tractions $\mathbf{t}$. The boundary $\partial\Omega$ consists of a portion Γ_u, on which the displacements $\mathbf{d}$ are prescribed, and a part Γ_t on which tractions $\mathbf{t}$ are prescribed. In the solid, there exist interconversions of mechanical, thermal and chemical energies. These processes are governed by the first law of

thermodynamics. To derive the energy equation describing the first law of thermodynamics we start with the equation of equilibrium

$$\nabla \cdot \boldsymbol{\sigma} + \rho \mathbf{b} = \rho \ddot{\mathbf{u}} \ , \tag{1}$$

where $\boldsymbol{\sigma}$ is the Cauchy stress and ρ is the density. Forming a scalar product with the velocity $\dot{\mathbf{u}}$, and integrating over the body

$$\int_{\Omega} (\nabla \cdot \boldsymbol{\sigma} + \rho \mathbf{b} - \rho \ddot{\mathbf{u}}) \cdot \dot{\mathbf{u}} \, \mathrm{d}x = 0 \ , \tag{2}$$

one can easily show

$$\underbrace{\int_{\Omega} \nabla \dot{\mathbf{u}} : \boldsymbol{\sigma} \, \mathrm{d}x}_{\frac{\mathrm{d}\mathscr{E}}{\mathrm{d}t}} + \underbrace{\int_{\Omega} \rho \ddot{\mathbf{u}} \cdot \dot{\mathbf{u}} \, \mathrm{d}x}_{\frac{\mathrm{d}K}{\mathrm{d}t}} = \underbrace{\int_{\Omega} \rho \mathbf{b} \cdot \dot{\mathbf{u}} \, \mathrm{d}x + \int_{\partial\Omega} \boldsymbol{\sigma} \cdot \mathbf{n} \cdot \dot{\mathbf{u}} \, \mathrm{d}s}_{\frac{\mathrm{d}W}{\mathrm{d}t}} \ . \tag{3}$$

By further manipulations one can write the time rate of kinetic energy as

$$\frac{\mathrm{d}K}{\mathrm{d}t} = \int_{\Omega} \rho \ddot{\mathbf{u}} \cdot \dot{\mathbf{u}} \, \mathrm{d}x \ . \tag{4}$$

For a thermomechanical continuum it is customary to express the time rate of change of internal energy by

$$\frac{\mathrm{d}\mathscr{E}}{\mathrm{d}t} = \frac{\mathrm{d}}{\mathrm{d}t} \int_{\Omega} \rho e \, \mathrm{d}x = \int_{\Omega} \rho \frac{\mathrm{d}e}{\mathrm{d}t} \mathrm{d}x \ , \tag{5}$$

where e is the internal energy per unit mass. Heat conduction as well as thermal source effects are included by

$$\frac{\mathrm{d}S}{\mathrm{d}t} \stackrel{\mathrm{def}}{=} \underbrace{-\int_{\partial\Omega} \mathbf{g} \cdot \mathbf{n} \, \mathrm{d}s}_{\text{conduction}} + \underbrace{\int_{\Omega} \rho z \, \mathrm{d}x}_{\text{sources}} \ , \tag{6}$$

where $\mathbf{g}$ is the heat flux per unit area per unit time and z is the heat influx per unit mass due to sources (possibly external sources or chemical reactions). This leads to

$$\frac{\mathrm{d}K}{\mathrm{d}t} + \frac{\mathrm{d}\mathscr{E}}{\mathrm{d}t} = \frac{\mathrm{d}W}{\mathrm{d}t} + \frac{\mathrm{d}S}{\mathrm{d}t} \ , \tag{7}$$

or, explicitly, the local form can be written

$$\rho \dot{e} = \boldsymbol{\sigma} : \nabla \dot{\mathbf{u}} - \nabla \cdot \mathbf{g} + \rho z \ . \tag{8}$$

Therefore, if $\rho \dot{e} = \rho \mathscr{H} \dot{\theta}$, where $\mathscr{H}$ is the heat capacity per unit mass, and $\dot{\theta}$ is the rate of temperature change (θ is the absolute temperature), then

$$\nabla \cdot \mathbf{g} = -\rho \dot{e} + \rho z + \boldsymbol{\sigma} : \nabla \dot{\mathbf{u}} = -\rho \mathscr{H} \dot{\theta} + \rho z + \boldsymbol{\sigma} : \nabla \dot{\mathbf{u}} \ . \tag{9}$$

Here, ρz represents mechanical energy losses during corrosion, for example, $\rho z > 0$ for all $\mathbf{x} \in \Omega$ undergoing chemical attack.

Remark: This phenomenological model does not account for losses or gains in mass due to chemical reactions. The material is assumed to change properties but the mass remains the same. Classical models for changes in the overall mass can be found in [1–3] or [4].

3
Model for corrosive species accumulation

An observed phenomenon in the diffusion of a small species in a solid is that of accumulation in regions of relatively low hydrostatic pressure. A simple constitutive model of such a

phenomenon, relating the flux of a small solute diffusing in a stressed solid, is given by the modified form of Fick's law incorporating the effects of pressure and pressure gradients into the diffusion equation, see [5–12],

$$\mathbf{F} = -\mathbf{D} \cdot (\nabla c - \alpha \varpi \nabla c - \gamma c \nabla \varpi) \quad \gamma, \alpha \geq 0 \ , \tag{10}$$

where c is the concentration of the solute and where ϖ is the volumetric strain, which under infinitesimal deformations is tr $\boldsymbol{\epsilon}$. One can argue on the basis of statistical mechanics that the diffusivity $\mathbf{D}$ $(\mathrm{m}^2/\mathrm{sec})$ must be positive definite in order to coincide with observed phenomena, i.e. a diffusing species is attracted to regions of relatively lower concentration under stress-free conditions. In the most general case, $\mathbf{D}$ is considered a second order tensor. The effect of the extra terms are as follows:

- $\alpha \varpi \nabla c$; the species are repelled from regions where the concentration is high and the volumetric strain gradients are negative
- $\gamma c \nabla \varpi$; the species accumulate in regions where the concentration is high and the volumetric gradients are positive.

It is clear that such a model can lead to sharp concentration fronts, which is a desired effect since it is experimentally observed. Upon substituting this relation into the conservation law,

$$\dot{c} + \nabla \cdot \mathbf{F} = 0 \ ,$$

one obtains the following equation governing the diffusion of a dilute solute in a stressed solid:

$$\dot{c} = \nabla \cdot [\mathbf{D} \cdot (\nabla c - \alpha \varpi \nabla c - \gamma c \nabla \varpi)] \ . \tag{11}$$

The diffusivity of a material has a well-known relationship to the temperature, namely the Arhennius form

$$\mathbf{D} = \mathbf{D}^0 \mathrm{e}^{-\frac{Q}{R\theta}}$$

where $\mathbf{D}^0$ is a spatially heterogeneous diffusivity tensor at a reference temperature, Q is the activation energy for solute motion per mole of diffusive species and R is the universal gas constant.

3.1
Transport relations

If we employ the Fourier ansatz, for heat conduction

$$\mathbf{g} = -\mathbf{K} \cdot \nabla \theta$$

$\mathbf{K}$ being the thermal conductivity, a second order tensor in the most general case and positive definite by the second law of thermodynamics, we have the following relations:

$$\begin{aligned} &-\nabla \cdot \mathbf{F} = \dot{c} \ , \quad \text{(mass conservation)} \\ &-\nabla \cdot \boldsymbol{\sigma} = \rho \mathbf{b} - \rho \ddot{\mathbf{u}} \ , \quad \text{(momentum balance)} \\ &-\nabla \cdot \mathbf{g} = \rho \mathscr{H} \dot{\theta} - \boldsymbol{\sigma} : \nabla \dot{\mathbf{u}} - \rho z \ , \quad \text{(first law of thermodynamics)} \end{aligned} \tag{12}$$

where c is the concentration of the diffusing corrosive solute (per unit volume),

$$\mathbf{F} = \mathbf{F}(\mathbf{u}, \theta, c), \quad \boldsymbol{\sigma} = \boldsymbol{\sigma}(\mathbf{u}, \theta, c) \quad \text{and} \quad \mathbf{g} = \mathbf{g}(\mathbf{u}, \theta, c) \ .$$

3.2
Phenomenological degradation

As we have mentioned in the introduction, the macroscopic loss in material stiffness suggests an irreversible phenomenological model for mesoscopic degradation:

$$\begin{aligned} &\text{for each } x \in \Omega \text{ if } c > c_{\text{crit}} \text{ at a moment in time } t, \text{ then } \mathbb{E}|_{(t+\delta t)} \leq \mathbb{E}|_{(t)} \\ &\mathbf{0} < \mathbb{E}|_{(t+\delta t)} \leq \mathbb{E}|_{(t)} \leq \mathbb{E}|_{(t=0)} \quad \forall x \in \Omega \ . \end{aligned} \tag{13}$$

The notation $\mathbb{E}|_{(t+\delta t)} \leq \mathbb{E}|_{(t)}$ means that the eigenvalues of $\mathbb{E}|_{(t+\delta t)} - \mathbb{E}|_{(t)}$ are negative semi-definite. In the literature, a variety of models employing exponential laws for mechanical

damage growth have been successful in matching experiments, see for example [13]. With this in mind, an expedient model is:

$$\text{for each } x \in \Omega \text{ if } c > c_{\text{crit}} \text{ at a moment in time } t, \text{ then } \mathbb{E} \to \mathbb{E}e^{-\beta\frac{c}{c_{\text{crit}}}} \quad 0 < \beta,$$
$$\text{restriction: } \mathbf{0} < \mathbb{E}|_{(t+\delta t)} \leq \mathbb{E}|_{(t)} \leq \mathbb{E}|_{(t=0)} \quad \forall x \in \Omega \ . \tag{14}$$

With this model, increasing β increases the detrimental effects of the corrosive. Here, β is a material constant, and we refer to it as the corrosion parameter. From the physical point of view, the corrosion parameter β and the critical amount of the corrosive c_{crit} should be selected to match realistic damage rates observed in laboratory experiments. This model is irreversible, in the sense that if the corrosive leaves after a period of time, the material does not return to its original state. We assume that the energy lost from the weakening of the mechanical properties is in the form of heat, in other words, using the previous notation, the source term in the energy equation becomes:

$$\text{for each } x \in \Omega \text{ if } c > c_{\text{crit}} \text{ at a moment in time } t, \text{ then: } \rho z = \zeta\rho\sqrt{\dot{\mathbb{E}} : \dot{\mathbb{E}}},$$
$$\text{for each } x \in \Omega \text{ if } c \leq c_{\text{crit}} \text{ at a moment in time } t, \text{ then: } \rho z = 0 \ , \tag{15}$$

where ζ is a measurable material constant, which represents a constant of conversion of mechanical properties into heat energy. This is merely one of many possible choices for a phenomenological corrosion law.

4
Widespread example: hydrogen damage

The relatively small atomic form of hydrogen allows it to easily penetrate most solid structures. Primarily, because molecular hydrogen is too large to diffuse from the surface into the metal lattice, it is usually assumed that atomic hydrogen must be formed on the surface of a structure. The atomic form of hydrogen can occur in a variety of ways: corrosion processes, electroplating, as a waste product in chemical reactions of combustion cycles, etc. The mechanisms of hydrogen degradation are numerous. A prominent example is the formation of brittle hydrides which inhibit grain sliding during deformation, thus embrittling the material. Another example is blistering caused by hydrogen accumulating, reacting and causing high pressure which results in localized rupture. Both premature failure and loss of strength are usually observed in tensile tests of metals exposed to hydrogen gas. There are a variety of view points as to the actual subcontinuum mechanism for hydrogen damage in metallic solids. However, there are some commonly agreed upon aspects. In general, it is believed that hydrogen damage in metallic materials occurs because hydrogen absorption at highly stressed sites lowers the surface energy required for intergranular microcracks to grow. There are two classical schools of thought, both advocating a microinterface (intergranular) decohesion model. The first proposes that the decohesion occurs at the highest stress triaxiality (hydrostatic) region, see [14] and [15], while the second is based on hydrogen-induced microplasticity models, see [16] and [17]. Loosely speaking, hydrogen reduces the bonding energy of the metal lattice sufficiently enough to allow intergranular cracking. There are numerous works in the area of intergranular decohesion and hydrogen damage, and we refer the reader to [18–28]. From a structural analyst's point of view, regardless of the exact intergranular failure mechanism, the important effect is that the grains are observed to separate, and that the likelihood of decohesion is directly related to the amount of hydrogen present.

4.1
Analysis of intergranular decohesion: a method to determine the phenomenological corrosion parameters

Intergranular crack growth rates in the presence of hydrogen have been reported in the literature to be on the order of $10^{-8} - 10^{-7}$ m/sec for commonly used metallic solids such as steel, [20], [25], indicating that an intergranular crack jumps approximately 1 micron every 20 seconds. Experimentally, this is determined by locating crack arrest markings with a scanning electron microscope. One way to determine the corrosion parameter β for our degradation model, is to consider decohesion of the intergranular interfaces. In a relevant study, [29], the decohesion was modeled as a result of hydrogen reaction with internal constituents, carbides in carbon steels, which form high-pressure microvoids filled with methane gas. These pressurized microvoids grow until they coalesce and form intergranular cracks, (Fig. 2). It is the

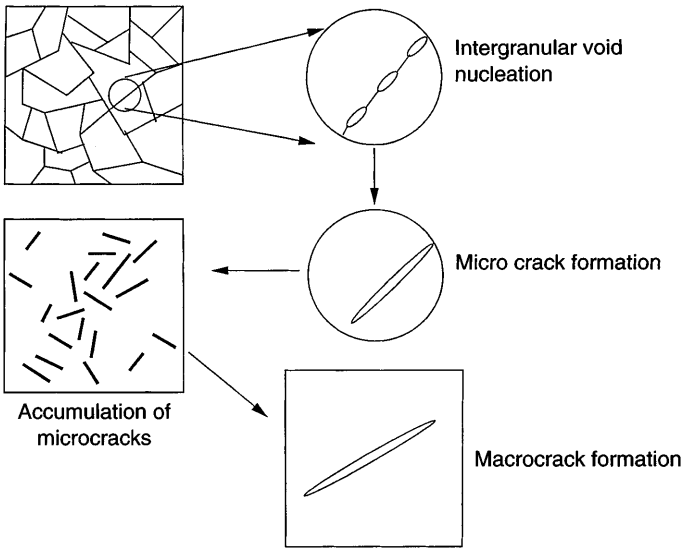

Fig. 2. Progressive void nucleation, microcrack formation and macrocrack formation

immediate objective of this Section to investigate the effects of stress on the diffusion of hydrogen from a macroscopic crack containing hydrogen, which has resulted from a such corrosion process.

4.2
Analysis at a crack tip

A close-up view of a single grain is shown in Fig. 3. To model intergranular decohesion, we consider an idealization of an intergranular crack with hydrogen atoms adsorbed at the root. We motivate a blunted crack model both physically and mathematically, by considering an initially sharp crack under a remote uniaxial loading causing the stress field in the solid. The usual linearly elastic mode I crack solution (opening mode) in an infinite two-dimensional domain under uniaxial tension is considered for plane states. The elastic stress field in mode I loading for in-plane stress near the crack tip can be expressed as

$$\sigma_{ij} = \frac{K_I}{\sqrt{2\pi r}} f_{ij}(\theta) \ , \tag{16}$$

where f_{ij} is a known function of θ and K_I is at this point still unknown, since the body and loading are unknown. Here, polar coordinates (r, θ) from the origin of the crack tip are used. If K_I is known, then all stresses can be determined. It is usual to express $K_I = \eta\sigma\sqrt{a}$, where a is the half-length of the crack, σ is the remote stress and η is unknown. For an infinite planar domain under remote uniaxial loading we have (with $\eta = \sqrt{\pi}$)

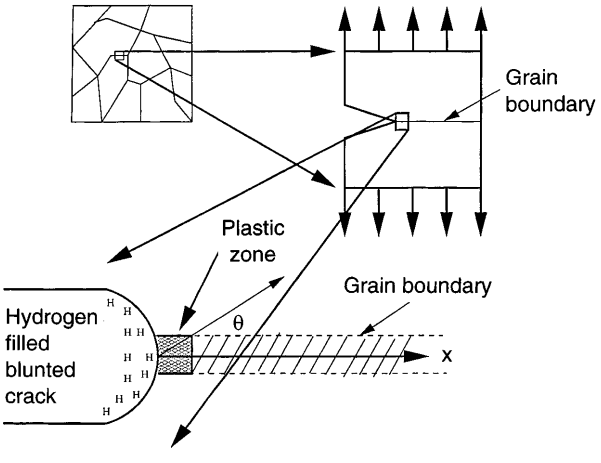

Fig. 3. A close-up view of a blunted intergranular crack

$$\sigma_{xx} = \frac{K_I}{\sqrt{2\pi r}} \cos\frac{\theta}{2}\left(1 - \sin\frac{\theta}{2}\sin\frac{3\theta}{2}\right),$$

$$\sigma_{yy} = \frac{K_I}{\sqrt{2\pi r}} \cos\frac{\theta}{2}\left(1 + \sin\frac{\theta}{2}\sin\frac{3\theta}{2}\right),$$

$$\sigma_{xy} = \frac{K_I}{\sqrt{2\pi r}} \sin\frac{\theta}{2}\cos\frac{\theta}{2}\cos\frac{3\theta}{2}, \tag{17}$$

$$\sigma_{zz} = v(\sigma_{xx} + \sigma_{yy}) \quad \text{for plane strain},$$

$$\sigma_{zz} = 0 \quad \text{for plane stress},$$

$$\sigma_{xz} = \sigma_{yz} = 0 \ ,$$

where v is the material Poisson ratio. Such an analysis is classical, involving Airy stress functions and standard complex variable methods, see [30].

4.2.1 Observations

Along the $\theta = 0$ axis, the pressure gradients behave as $\nabla P = \mathcal{O}(r^{-\frac{3}{2}})$. It is important to realize that the pressure is harmonic, i.e. $\nabla^2 P = 0$, in the case of constant body forces and provided the fields are twice differentiable. This is a direct result of the Beltrami-Mitchell formulation of elasticity. The result does hold for plastic responses under the assumption that the dilatational stresses are not affected by plastic deformations (J_2 theory).

Suppose we restrict the diffusion equation to a single direction (one-dimensional problem). By inserting the relations in Eqs. (17) into Eq. (11), the general relations collapse to

$$c'' + \frac{Ac'}{x^{\frac{3}{2}}} = 0 \ ,$$

where A is a constant. Such a problem is ill-posed since the singularity is not integrable, i.e. $\int_\Omega c \, dx = \infty$. In order to extract some meaningful information we must consider that the material will plastify ahead of the crack tip. The resulting solution is therefore regularized. A rough idea of the plastic zone size and shape can be determined by finding all points, where $\sqrt{\boldsymbol{\sigma}' : \boldsymbol{\sigma}'} \geq \sigma_{\text{yield}}$. The plastic zone for the plane strain condition is given by

$$r_p = \max\left[\frac{K_I^2}{2\pi\sigma_{\text{yield}}^2}\cos^2\frac{\theta}{2}\left(1 - 2v + \sin\frac{\theta}{2}\right)^2, \ \frac{K_I^2}{2\pi\sigma_{\text{yield}}^2}\cos^2\frac{\theta}{2}\right] \ , \tag{18}$$

while for plane stress

$$r_p = \frac{K_I^2}{2\pi\sigma_{\text{yield}}^2}\left[\cos\frac{\theta}{2}\left(1 + \sin\frac{\theta}{2}\right)\right]^2 \ . \tag{19}$$

A simple approximation is to assume that the pressure is constant in the plastic zone, and to use the elastic field outside of the plastic zone, see Figs. 4 and 5. It is clear that such a model will

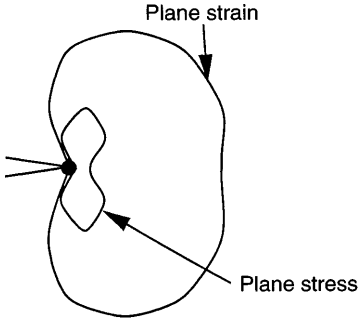

Fig. 4. A close-up of the plastic zone shapes ahead of a crack

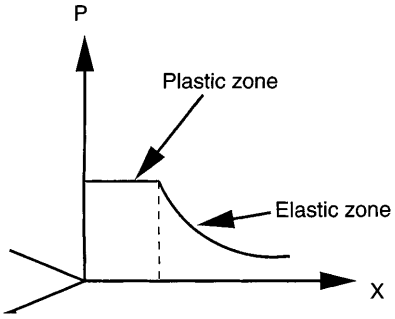

Fig. 5. An elasto-plastic pressure field ahead of the crack

force accumulation at the plastic-elastic interface. This has been experimentally and computationally observed in [19], [23–28]. The usual assumption is that the crack will advance when a critical amount of hydrogen has been absorbed in the plastic zone, and the material ahead of the crack is sufficiently weakened.

4.3
Inverse problem for the corrosion parameter

A way to determine the corrosion parameter β is by finding the minimum of β that will produce complete degradation of the material in the plastic zone in 20 seconds. In other words one must find the minimum of β that achieves a sufficiently weakened intergranular strip material, measured by the following

$$\text{Intergranular strip losses} \overset{\text{def}}{=} \underbrace{\left| \frac{\langle E_s^O \rangle_\Omega - \langle E_s^C \rangle_\Omega}{\langle E_s^O \rangle_\Omega} \right|}_{\text{in } 1\mu\text{m}} \leq 1 \ , \tag{20}$$

where E_s^C is the time-dependent spatially varying corroded Young's modulus and E_s^O is the original uncorroded Young's modulus of the intergranular strip. Accordingly, we solve

$$-\nabla \cdot \mathbf{F} = \dot{c}, \quad \mathbf{F} = -\mathbf{D} \cdot (\nabla c - \alpha \varpi \nabla c - \gamma c \nabla \varpi), \quad \mathbf{D} = \mathbf{D}^0 \mathrm{e}^{-\frac{Q}{R\theta}} \ , \tag{21}$$

along a one-dimensional strip with a constant temperature field by the finite difference method. The pressure field is taken to be a constant in the plastic zone, dictated by the yield stress. In the elastic zone, the pressure is harmonic and is governed by Eqs. (17). Quantitative results are given in Table 1. The results are mesh-independent, i.e we successively refined the time and spatial steps until no change in the solution occurred to 5 significant digits We employ $\beta = 0.001$ and $c_{\text{crit}} = 1.0$ as a realistic combination of parameters for the RVE scale simulations.

5
Numerical and analytical approximations

In multiphase media, a prevalent damage mechanism is the phenomenon of corrosive species trapping. This degradation mechanism frequently occurs when two phases of varying diffusivities are present, see [20] for comments on hydrogen trapping. For example, when a high-diffusivity matrix is present, the corrosive initially diffuses through quickly, and remains trapped between the denser low diffusivity particulate phases. After initial absorption by the matrix, the corrosive is trapped between the low diffusivity particles, whereby it destroys the material. In an attempt to simulate such trapping, we consider two-phase dispersed-phase

Table 1. The corrosion parameter for a given critical amount of hydrogen in 20 seconds; $\kappa = 162\,\text{GPa}$, $\mu = 75.8\,\text{GPa}$, $\sigma_{\text{yield}} = 100\,\text{MPa}$, grain boundary length = 10 μm and plastic zone size 1 μm, (values for homogeneous steel; for other parameters s. Table 2)

c_{crit}	β	$\left\langle \frac{E^O - E^C}{E^O} \right\rangle_{1\,\mu m}$
0.5	0.00001	0.019
0.5	0.0001	0.177
0.5	0.001	0.859
1.0	0.00001	0.009
1.0	0.0001	0.093
1.0	0.001	0.624

particulate composites. For moderate contrasts in the particle and matrix material, the sample must contain several particles to be statistically representative. We consider an idealization of a microstructure that would be susceptible to trapping: a cube of material with a heterogeneous two-phase particulate isotropic random block microstructure. The cubical domain is subdivided into subblocks of uniform size. They are randomly assigned either hard (particulate) or soft (matrix) material values (a random 3-D "checkerboard", Fig. 6), and then the hard subblocks are scaled down, Fig. 7, forming interparticle ligaments vulnerable to the trapping phenomena. One can consider the hard subblocks to be the stiffer, harder to penetrate, particles, while the surrounding material to be the softer, more permeable, matrix. Numerical results are presented below.

5.1
Approximation schemes for thermo/chemical/mechanical coupling

In order to reduce the complexity of the computations, we employ some classical approximations for the mechanical fields. The internal mechanical fields will be approximated from above and below in a certain sense. Thereafter, we can construct the local pressure-dependent diffusive coefficients for the mass conservation equation throughout the body as well as the mechanical contributions to the energy equation. In order to approximate the internal mechanical fields, we employ standard micro/macroenergy arguments. As we have stated in the introduction, macroscopic, aggregate or "effective" constitutive relations of a microheterogeneous material are usually computed from a relation between averaged stress and strain in an RVE with volume $|\Omega|$, s Sec. I. However, for the relation between averages to make sense, i.e. to be statistically representative, the sample size may have to be quite large relative to the intrinsic length scales of the microstructure. The size requirements placed on the RVE can be stated concisely by the following micro/macroenergy equality:

$$\langle \boldsymbol{\sigma} : \boldsymbol{\epsilon} \rangle_{\Omega} = \langle \boldsymbol{\sigma} \rangle_{\Omega} : \langle \boldsymbol{\epsilon} \rangle_{\Omega} \ ,$$

known as Hill's condition, [31]. For a heterogeneous body, two important loadings that fall under Hill's condition are

$$\begin{aligned} &(1)\ \mathbf{u}|_{\partial\Omega} = \mathbf{S}\cdot\mathbf{x} \Rightarrow \langle \boldsymbol{\epsilon} \rangle_{\Omega} = \mathbf{S} \ , \\ &(2)\ \mathbf{t}|_{\partial\Omega} = \mathbf{T}\cdot\mathbf{n} \Rightarrow \langle \boldsymbol{\sigma} \rangle_{\Omega} = \mathbf{T} \ , \end{aligned} \tag{22}$$

where $\mathbf{S}$ and $\mathbf{T}$ are constant strain and stress tensors, respectively. Note, that $\boldsymbol{\epsilon}$ is a special linear boundary displacement. Clearly, for Hill's condition to be realizable in a sample within a macroscopic structure under possibly nonuniform external loading, the sample must be large enough to have negligibly small field fluctuations relative to its size. Under Hill's condition, it is possible to relate $\mathbb{E}^*$ to the approximations $\langle \mathbb{E} \rangle_{\Omega}$ and $\langle \mathbb{E}^{-1} \rangle_{\Omega}^{-1}$, due to Voigt (constant strain throughout the body) and Reuss (constant stress throughout the body), respectively. As a simple calculation reveals the above relation implies $\langle \mathbb{E}^{-1} \rangle_{\Omega}^{-1} \leq \mathbb{E}^* \leq \langle \mathbb{E} \rangle_{\Omega}$. It is well known that one can relate the upper bound to an assumed constant strain field (Voigt) within the RVE, $\boldsymbol{\epsilon} = \boldsymbol{\epsilon}^0$,

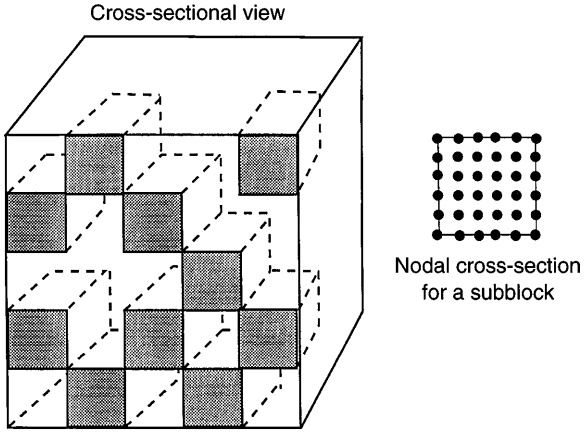

Fig. 6. The model problem before scaling down the microstructure to simulate hydrogen trapping

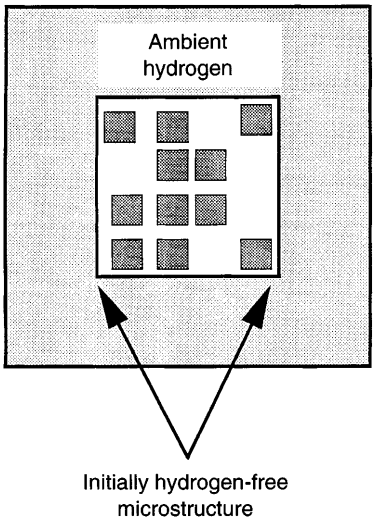

Fig. 7. Cross section after the scaling down of the particles

$$\langle \boldsymbol{\sigma} \rangle_\Omega = \langle \mathbb{E} : \boldsymbol{\epsilon} \rangle_\Omega = \langle \mathbb{E} \rangle_\Omega : \boldsymbol{\epsilon}^0 \Rightarrow \mathbb{E}^* = \langle \mathbb{E} \rangle_\Omega \ . \tag{23}$$

Alternatively, an assumed constant stress field (Reuss), $\boldsymbol{\sigma} = \boldsymbol{\sigma}^0$ yields

$$\langle \boldsymbol{\epsilon} \rangle_\Omega = \langle \mathbb{E}^{-1} : \boldsymbol{\sigma} \rangle_\Omega = \langle \mathbb{E}^{-1} \rangle_\Omega : \boldsymbol{\sigma}^0 \Rightarrow \mathbb{E}^* = \langle \mathbb{E}^{-1} \rangle_\Omega^{-1} \ . \tag{24}$$

Therefore, the Reuss and Voigt fields provide the two extremes of possible elastic microfield behavior. The first produces kinematically inadmissible fields, while the second produces statically inadmissible fields. We will use these extreme conditions to construct all approximations. Accordingly, the numerical simulations must be performed twice, once with the Voigt approximation and once with the Reuss approximation. If we assume uniform pressure loading on the boundary of the sample, we obtain

$$\boldsymbol{\sigma} \cdot \mathbf{n}|_{\partial\Omega} = \begin{bmatrix} \pm P^0 & 0 & 0 \\ 0 & \pm P^0 & 0 \\ 0 & 0 & \pm P^0 \end{bmatrix} \begin{bmatrix} n_1 \\ n_2 \\ n_3 \end{bmatrix}, (+ \text{ stands for compression, } - \text{ for tension}) \ , \tag{25}$$

which yields $\langle P \rangle_\Omega = P^0$; this can be proven by a simple integration by parts, and is usually referred to as the "average stress theorem". One arrives at

$$\begin{aligned} &\text{Reuss} : P = -3\kappa \frac{\operatorname{tr} \boldsymbol{\epsilon}}{3} = \text{constant} \Rightarrow P = P^0 \ , \\ &\text{Voigt} : \frac{\operatorname{tr} \boldsymbol{\epsilon}}{3} = -\frac{P}{3\kappa} = \text{constant} \Rightarrow P = \kappa \frac{P^0}{\langle \kappa \rangle_\Omega} \ . \end{aligned} \tag{26}$$

In accordance with the approximations in Eqs. (26), we focus on a normalized loss in the Young's modulus, $E = 9\kappa\mu/(3\kappa + \mu)$, as a function of time. Here, μ is the spatially variable shear modulus. Under our assumptions thus far, measures for the losses in the macroscopic response are

$$\begin{aligned} \text{Reuss losses} = \quad & \mathscr{L}_{\mathrm{R}} \stackrel{\text{def}}{=} \left| \frac{\langle (\mathrm{E}^{\mathrm{O}})^{-1} \rangle_\Omega^{-1} - \langle (\mathrm{E}^{\mathrm{C}})^{-1} \rangle_\Omega^{-1}}{\langle (\mathrm{E}^{\mathrm{O}})^{-1} \rangle_\Omega^{-1}} \right|, \\ \text{Voigt losses} = \quad & \mathscr{L}_{\mathrm{V}} \stackrel{\text{def}}{=} \left| \frac{\langle \mathrm{E}^{\mathrm{O}} \rangle_\Omega - \langle \mathrm{E}^{\mathrm{C}} \rangle_\Omega}{\langle \mathrm{E}^{\mathrm{O}} \rangle_\Omega} \right| \ , \end{aligned} \tag{27}$$

where E^C is the time-dependent spatially varying corroded Young's modulus and E^O is the original uncorroded, spatially variable Young's modulus.

5.1.1
Simple updating scheme

The physical process is clear in such problems: (1) the diffusing species penetrates, (2) the reactions occur, (3) the mechanical properties change and (4) the heat is released. Numerically,

the irreversible term $\rho z(\boldsymbol{\sigma}, \nabla \mathbf{u})$ and the corresponding corrosion of $\mathbb{E}$ are updated only at the end of each time step. The time steps are chosen to correspond to the observed finite time for granular decohesion to occur. Therefore, throughout a fixed time step $(t + \delta t)$, $\rho z = \rho z|_t$ and $\mathbb{E} = \mathbb{E}|_t$. With these approximations, we can use the following algorithm at each time step: (1) solve the energy equation; (2) solve the diffusion equation with the temperature fields; (3) compute the corrosion of the material and (4) update the mechanical fields.

5.2
Numerical solution of the mass conservation (diffusion) equation

We employ standard implicit finite difference schemes to compute the diffusive behavior of corrosive species. To make the notation somewhat easier to follow we define the following:

$$\mathbf{F} = -\mathbf{D} \cdot (\nabla c - \alpha \varpi \nabla c - \gamma c \nabla \varpi) = -\tilde{\mathbf{D}} \cdot \nabla c + \mathbf{D} \cdot (\gamma c \nabla \varpi) \ , \tag{28}$$

where

$$\tilde{\mathbf{D}} \stackrel{\text{def}}{=} \mathbf{D}(1 - \alpha\varpi), \quad \mathbf{D}(x, y, z) = \mathbf{D}^0(x, y, z) \mathrm{e}^{-\frac{Q(x,y,z)}{R\theta(x,y,z)}} \ .$$

We assume that $\mathbf{D}$ is isotropic, but spatially variable. Therefore, $\mathbf{D}$ can be represented by a scalar function, D. Using a seven-point finite difference stencil in three dimensions, the terms that appear in the governing differential equation are approximated as follows:

$$\tilde{D}\nabla c \approx \tilde{D}(x, y, z)\left(\tfrac{c(x+h,y,z)-c(x-h,y,z)}{2h}\mathbf{i} + \tfrac{c(x,y+h,z)-c(x,y-h,z)}{2h}\mathbf{j} + \tfrac{c(x,y,z+h)-c(x,y,z-h)}{2h}\mathbf{k}\right) \ , \tag{29}$$

where h is the uniform grid spacing for the x, y and z directions. Applying the difference formulas once again to the fluxes, we obtain

$$\begin{aligned}
\nabla \cdot (\tilde{D}\nabla c) \approx \frac{1}{4h^2} [&\tilde{D}(x + h, y, z)c(x + 2h, y, z) - \tilde{D}(x - h, y, z)c(x, y, z) \\
&- \tilde{D}(x + h, y, z)c(x, y, z) + \tilde{D}(x - h, y, z)c(x - 2h, y, z) \\
&+ \tilde{D}(x, y + h, z)c(x, y + 2h, z) - \tilde{D}(x, y - h, z)c(x, y, z) \\
&- \tilde{D}(x, y + h, z)c(x, y, z) + \tilde{D}(x, y - h, z)c(x, y - 2h, z) \\
&+ \tilde{D}(x, y, z + h)c(x, y, z + 2h) - \tilde{D}(x, y, z - h)c(x, y, z) \\
&- \tilde{D}(x, y, z + h)c(x, y, z) + \tilde{D}(x, y, z - h)c(x, y, z - 2h)] \stackrel{\text{def}}{=} \mathbb{d}_{\mathrm{I}}^2 c \ ,
\end{aligned} \tag{30}$$

and

$$\begin{aligned}
\nabla \cdot (Dc\gamma\nabla\varpi) \approx \frac{1}{4h^2} [&D(x + h, y, z)c(x + h, y, z)\gamma(x + h, y, z)\varpi(x + 2h, y, z) \\
&- D(x - h, y, z)c(x - h, y, z)\gamma(x - h, y, z)\varpi(x, y, z) \\
&- D(x + h, y, z)c(x + h, y, z)\gamma(x + h, y, z)\varpi(x, y, z) \\
&+ D(x - h, y, z)c(x - h, y, z)\gamma(x - h, y, z)\varpi(x - 2h, y, z) \\
&+ D(x, y + h, z)c(x, y + h, z)\gamma(x, y + h, z)\varpi(x, y + 2h, z) \\
&- D(x, y - h, z)c(x, y - h, z)\gamma(x, y - h, z)\varpi(x, y, z) \\
&- D(x, y + h, z)c(x, y + h, z)\gamma(x, y + h, z)\varpi(x, y, z) \\
&+ D(x, y - h, z)c(x, y - h, z)\gamma(x, y - h, z)\varpi(x, y - 2h, z) \\
&+ D(x, y, z + h)c(x, y, z + h)\gamma(x, y, z + h)\varpi(x, y, z + 2h) \\
&- D(x, y, z - h)c(x, y, z - h)\gamma(x, y, z - h)\varpi(x, y, z) \\
&- D(x, y, z + h)c(x, y, z + h)\gamma(x, y, z + h)\varpi(x, y, z) \\
&+ D(x, y, z - h)c(x, y, z - h)\gamma(x, y, z - h)\varpi(x, y, z - 2h)] \stackrel{\text{def}}{=} \mathbb{d}_{\mathrm{II}}^2 c \ .
\end{aligned} \tag{31}$$

The time-dependent term is approximated by a central difference approximation at $t + \delta t/2$, $\dot{c} \approx (c|_{t+\delta t} - c|_t)/\delta t$. The standard scheme for $0 < \Lambda < 1$ is as follows:

$$\underbrace{\Lambda(\mathbb{d}_{\mathrm{I}}^2 c - \mathbb{d}_{\mathrm{II}}^2 c)}_{\text{approximated at } t} + \underbrace{(1-\Lambda)(\mathbb{d}_{\mathrm{I}}^2 c - \mathbb{d}_{\mathrm{II}}^2 c)}_{\text{approximated at } t+\delta t} = \underbrace{\dot{c}}_{\text{approximated at } t+\delta t/2} . \tag{32}$$

The implicit nature of this approach allows us to take relatively large time steps compared to a direct explicit method. For more details see e.g. [32].

5.3
Frontal solver

For the considered problems, due to the microstructure the rapid fluctuations in the fields force the numerical mesh density to be quite high for sufficient accuracy. Because of this, simulations typically require a minimum of several thousand degrees of freedom, even for a relatively small problem. Such a system of equations must be solved at each time step, and thus can overwhelm most workstations, unless computationally efficient schemes are employed. The approach taken here is, at a fixed time step, to group together terms and apply the Successive Over Relaxation (SOR) iteration procedure in a moving front fashion. In this approach, all nodes behind the front have the updated SOR values, while those ahead have the previous iteration values, Fig. 8. This allows no zeros to be stored (no full matrix) in the iteration process. The approach is standard, see e.g. [33]. Grouping together terms, noting that all values of $c(x,y,z)$, where (x,y,z) are nodal coordinates of the discrete approximation, behind the front have the previous SOR iteration's values, we have, evaluated at the current time $t+\delta t$, on the front

$$A|_{t+\delta t} \stackrel{\text{def}}{=} -\left\{ \frac{1-\Lambda}{4h^2} [\tilde{D}(x+h,y,z) + \tilde{D}(x-h,y,z) + \tilde{D}(x,y+h,z) + \right.$$
$$\left. + \tilde{D}(x,y-h,z) + \tilde{D}(x,y,z+h) + \tilde{D}(x,y,z-h)] \right\} \Big|_{t+\delta t} - \frac{1}{\delta t} , \tag{33}$$

ahead of the front

$$B^{(1)}|_{t+\delta t} \stackrel{\text{def}}{=} \left\{ \frac{1-\Lambda}{4h^2} [\tilde{D}(x+h,y,z) c^{i-1\mathrm{SOR}}(x+2h,y,z) + \tilde{D}(x,y+h,z) c^{i-1\mathrm{SOR}}(x,y+2h,z) \right.$$
$$\left. + \tilde{D}(x,y,z+h) c^{i-1\mathrm{SOR}}(x,y,z+2h)] \right\} \Big|_{t+\delta t} - a^{(1)} \Big|_{t+\delta t} , \tag{34}$$

behind the front

$$B^{(2)}|_{t+\delta t} \stackrel{\text{def}}{=} \left\{ \frac{1-\Lambda}{4h^2} [\tilde{D}(x-h,y,z) c^{i\mathrm{SOR}}(x-2h,y,z) + \tilde{D}(x,y-h,z) c^{i\mathrm{SOR}}(x,y-2h,z) \right.$$
$$\left. + \tilde{D}(x,y,z-h) c^{i\mathrm{SOR}}(x,y,z-2h)] \right\} \Big|_{t+\delta t} - b^{(2)} \Big|_{t+\delta t} , \tag{35}$$

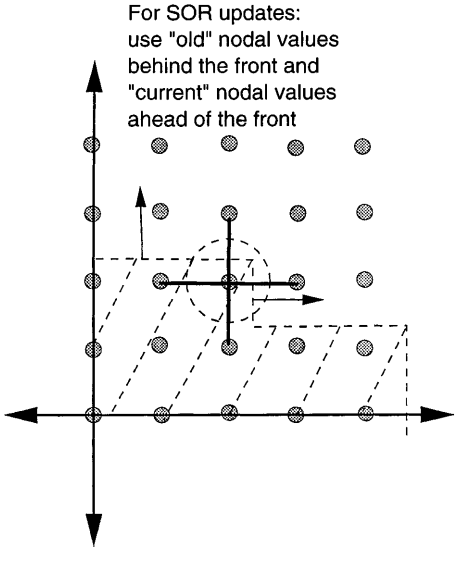

Fig. 8. The moving front corresponding to the SOR method

evaluated at the previous time t

$$R|_t \stackrel{\text{def}}{=} \Lambda(\mathbb{d}_{\mathrm{I}}^2 c)\Big|_t - \Lambda(\mathbb{d}_{\mathrm{II}}^2 c)\Big|_t + \frac{c(x,y,z)}{\delta t}\Big|_t \ , \tag{36}$$

where we have split the terms into those ahead of and behind the front

$$\begin{aligned} a^{(1)} \stackrel{\text{def}}{=} \frac{1-\Lambda}{4h^2}[&D(x+h,y,z)c(x+h,y,z)\gamma(x+h,y,z)\varpi(x+2h,y,z) \\ &- D(x+h,y,z)c(x+h,y,z)\gamma(x+h,y,z)\varpi(x,y,z) \\ &+ D(x,y+h,z)c(x,y+h,z)\gamma(x,y+h,z)\varpi(x,y+2h,z) \\ &- D(x,y+h,z)c(x,y+h,z)\gamma(x,y+h,z)\varpi(x,y,z) \\ &+ D(x,y,z+h)c(x,y,z+h)\gamma(x,y,z+h)\varpi(x,y,z+2h) \\ &- D(x,y,z+h)c(x,y,z+h)\gamma(x,y,z+h)\varpi(x,y,z)] \ , \end{aligned} \tag{37}$$

and

$$\begin{aligned} b^{(2)} \stackrel{\text{def}}{=} \frac{1-\Lambda}{4h^2}[&-D(x-h,y,z)c(x-h,y,z)\gamma(x-h,y,z)\varpi(x,y,z) \\ &+ D(x-h,y,z)c(x-h,y,z)\gamma(x-h,y,z)\varpi(x-2h,y,z) \\ &- D(x,y-h,z)c(x,y-h,z)\gamma(x,y-h,z)\varpi(x,y,z) \\ &+ D(x,y-h,z)c(x,y-h,z)\gamma(x,y-h,z)\varpi(x,y-2h,z) \\ &- D(x,y,z-h)c(x,y,z-h)\gamma(x,y,z-h)\varpi(x,y,z) \\ &+ D(x,y,z-h)c(x,y,z-h)\gamma(x,y,z-h)\varpi(x,y,z-2h)] \ . \end{aligned} \tag{38}$$

Therefore, the system of equations yields

$$(B^{(1)} + B^{(2)})|_{t+\delta t} + A|_{t+\delta t} c^{i,\mathscr{GS}}|_{t+\delta t} + R|_t = 0 \ . \tag{39}$$

The iterations may be compactly written as follows at a time step:

$$\begin{aligned} c^{i,\mathscr{SOR}}|_{t+\delta t} &= (1-\Omega)c^{i-1,\mathscr{SOR}}|_{t+\delta t} + \Omega c^{i,\mathscr{GS}}|_{t+\delta t} \ , \\ c^{i,\mathscr{GS}}|_{t+\delta t} &= -\frac{(B^{(1)} + B^{(2)})|_{t+\delta t} + R|_t}{A|_{t+\delta t}} \ , \end{aligned} \tag{40}$$

where i is the current SOR iterate value, $1 \le \Omega \le 2$ is the free relaxation parameter, $\mathscr{GS}$ denotes the standard Gauss-Seidel iteration without relaxation, Ω is a parameter that reduces the spectral radius of eigenvalues of the iteration matrix, see [34] for details. We will make specific choices for Ω later in the paper. The iterations are carried out until at each time step

$$\frac{\sum_{i=1}^{N} |c^{i+1} - c^i|}{\sum_{i=1}^{N} |c^{i+1}|} \le \text{tol} \ .$$

5.4
Energy equation solution

For the energy equation the numerical procedure is quite similar to that for the diffusion equation. Using a seven-point finite difference stencil in three dimensions, the terms that appear in the governing differential equation are approximated as follows (assuming K is isotropic):

$$K\nabla\theta \approx K(x,y,z)\left(\frac{\theta(x+h,y,z)-\theta(x-h,y,z)}{2h}\mathbf{i} + \frac{\theta(x,y+h,z)-\theta(x,y-h,z)}{2h}\mathbf{j} + \frac{\theta(x,y,z+h)-\theta(x,y,z-h)}{2h}\mathbf{k}\right) \ , \tag{41}$$

where h is the uniform grid spacing for the x, y and z directions. Applying the difference formulas once again to the fluxes, we obtain

$$\begin{aligned}\nabla \cdot (K\nabla\theta) \approx \frac{1}{4h^2}[&K(x+h,y,z)\theta(x+2h,y,z) - K(x-h,y,z)\theta(x,y,z)\\ &- K(x+h,y,z)\theta(x,y,z) + K(x-h,y,z)\theta(x-2h,y,z)\\ &+ K(x,y+h,z)\theta(x,y+2h,z) - K(x,y-h,z)\theta(x,y,z)\\ &- K(x,y+h,z)\theta(x,y,z) + K(x,y-h,z)\theta(x,y-2h,z)\\ &+ K(x,y,z+h)\theta(x,y,z+2h) - K(x,y,z-h)\theta(x,y,z)\\ &- K(x,y,z+h)\theta(x,y,z) + K(x,y,z-h)\theta(x,y,z-2h)] \stackrel{\text{def}}{=} \mathbb{d}^2\theta \ . \end{aligned} \tag{42}$$

The time-dependent term is approximated by a central difference approximation at $t + \delta t/2$, $\dot{\theta} \approx \theta|_{t+\delta t} - \theta|_t/\delta t$. The standard Crank-Nicolson scheme for $0 < \Lambda < 1$ is as follows, with the coupling terms treated as fixed loads:

$$\underbrace{\Lambda\mathbb{d}^2\theta}_{\text{approximated at } t} + \underbrace{(1-\Lambda)\mathbb{d}^2\theta}_{\text{approximated at } t+\delta t} = \underbrace{\rho\mathscr{H}\dot{\theta}}_{\text{approximated at } t+\frac{\delta t}{2}} - \underbrace{(\rho z)}_{\text{approximated at } t} - \underbrace{(\boldsymbol{\sigma} : \nabla\dot{\mathbf{u}})}_{\text{approximated at } t} \ , \tag{43}$$

where

$$\nabla\dot{\mathbf{u}} \approx \frac{\nabla\mathbf{u}|_t - \nabla\mathbf{u}|_{t-\delta t}}{\delta t} \ . \tag{44}$$

Grouping together terms evaluated at the current time $t + \delta t$ on the front we have

$$\begin{aligned}A|_{t+\delta t} \stackrel{\text{def}}{=} -\Bigg\{&\frac{1-\Lambda}{4h^2}[K(x+h,y,z) + K(x-h,y,z) + K(x,y+h,z)\\ &+ K(x,y-h,z) + K(x,y,z+h) + K(x,y,z-h)]\Bigg\}\Bigg|_{t+\delta t}\\ &- \frac{\rho(x,y,z)K(x,y,z)}{\delta t} \ , \end{aligned} \tag{45}$$

ahead of the front

$$\begin{aligned}B^{(1)}|_{t+\delta t} \stackrel{\text{def}}{=} \Bigg\{&\frac{1-\Lambda}{4h^2}[K(x+h,y,z)\theta^{i-1\text{SOR}}(x+2h,y,z) + K(x,y+h,z)\theta^{i-1\text{SOR}}(x,y+2h,z)\\ &+ K(x,y,z+h)\theta^{i-1\text{SOR}}(x,y,z+2h)]\Bigg\}\Bigg|_{t+\delta t} \ , \end{aligned} \tag{46}$$

behind the front

$$\begin{aligned}B^{(2)}|_{t+\delta t} \stackrel{\text{def}}{=} \Bigg\{&\frac{1-\Lambda}{4h^2}[K(x-h,y,z)\theta^{i\text{SOR}}(x-2h,y,z) + K(x,y-h,z)\theta^{i\text{SOR}}(x,y-2h,z)\\ &+ K(x,y,z-h)\theta^{i\text{SOR}}(x,y,z-2h)]\Bigg\}\Bigg|_{t+\delta t} \ , \end{aligned} \tag{47}$$

evaluated at the previous time t

$$R|_t \stackrel{\text{def}}{=} \Lambda\mathbb{d}^2\theta|_t + \left.\frac{\rho(x,y,z)K(x,y,z)\theta(x,y,z)}{\delta t}\right|_t \ , \tag{48}$$

and

$$L|_t \stackrel{\text{def}}{=} \underbrace{\rho z}_{\text{approximated at } t} + \underbrace{\boldsymbol{\sigma} : \nabla\dot{\mathbf{u}}}_{\text{approximated at } t} \ . \tag{49}$$

Therefore, the system of equations can be written as

$$(B^{(1)} + B^{(2)})|_{t+\delta t} + A|_{t+\delta t}\theta^{i,\mathscr{GS}}|_{t+\delta t} + R|_t + L|_t = 0 \ . \tag{50}$$

As for the diffusion equation, the iterations may be compactly written as follows at a time step:

$$\begin{aligned} \theta^{i,\mathscr{SOR}}|_{t+\delta t} &= (1-\omega)\theta^{i-1,\mathscr{SOR}}|_{t+\delta t} + \omega\theta^{i,\mathscr{GS}}|_{t+\delta t} \ , \\ \theta^{i,\mathscr{GS}}|_{t+\delta t} &= -\frac{(B^{(1)} + B^{(2)})|_{t+\delta t} + R|_t + L|_t}{A|_{t+\delta t}} \ . \end{aligned} \tag{51}$$

6
Numerical results

In the RVE simulations, we have taken the sample of material of the size $0.1\,\text{mm} \times 0.1\,\text{mm} \times 0.1\,\text{mm}$, containing 100 cubical particles, occupying 40.9% volume. This volume was determined by successively increasing the sample size, until the response did not change. Each particle has dimensions $14\,\mu\text{m} \times 14\,\mu\text{m} \times 14\,\mu\text{m}$. We have computed that the theoretical time to complete fracture, i.e. the time for an uninhibited crack to move through this distance, to be approximately $0.0001\,\text{m}/10^{-7}\,\text{m/s} = 1000$ seconds. The boundary conditions have been $c|_{\partial\Omega} = 1.0$ and $\theta|_{\partial\Omega} = 0$. No external heat was supplied. The properties of materials tested are shown in Table 2. A steel matrix is considered, with 2 trial microstructures. For simplicity, the diffusivity of the materials, which are solute-dependent, were taken to be those for hydrogen in steel measured in [20]. Trial 2 corresponds to a homogeneous material. We have chosen $c_{\text{crit}} = 1.0$ and $\beta = 0.001$. In our computations we have set $\Lambda = 0.5$ (corresponding to the Crank-Nicolson method), $\Omega = 1.5$ (a middle over-relaxation value) and an iterative tolerance of $\text{tol} = 10^{-6}$. For the given sample, meshes of a $38 \times 38 \times 38$ mesh density (54872 unknowns) have been used. Each set of simulations, a complete time history, took more than 10 minutes. A single HP-P1100 PC was used for all computations. Comparable hardware is available in most academic and industrial work places, and thus such simulations are easily achievable for other material parameter selections. It is clear from the simulations that, with this model, the tensile loading is more detrimental than the compressive loading. This effect was expected, since the tensile state "opens up" (dilatates) the material. However, the rise in temperature is a more complex issue, and no simple explanation encompasses all of the presented results. The only common feature to the presented load cases was the initial rise in temperature due to the initial large conversion of high (virgin) mechanical strength, Eq. (15), into heat.

7
Conclusions and future work

The presented results have provided some initial qualitative and quantitative information which we intend to use in the development of more advanced numerical approaches for the complete model with irregular microstructure, employing no analytical approximation of the internal mechanical fields. For the numerical simulations to be of any practical value, benchmarking of the results against experiments is necessary. Due to the continually degrading material, the microstructure becomes highly heterogeneous during the progressive corrosion stages. With the finite difference method, it is only possible to capture this behavior at nodal points, therefore the finite element method, which is integral based, is more advantageous, due to the fact that more material variations can be captured by Gauss points in the interior of each element. If we remove the analytical approximation of the mechanical fields, we must employ a fully staggered scheme at each time step, and this is under current investigation by the authors.

Table 2. Local material properties used in the simulations; Q = 7000 Nm/mole, $\mathscr{H}$ = 345.17 N/deg s, $\alpha = 1 \times 10^{-10}$ m^2/N, $\gamma = 3 \times 10^{-6}$ Nm/deg m^3

Material	κ(Gpa)	μ(Gpa)	D^0 (m/sec^2)	K (N/deg sec)	ρ (kg/m^3)
Steel	162	75.8	1.2×10^{-13}	61.92	7864.84
Trial 1	1620.	758.	$.12 \times 10^{-13}$	619.2	78648.4
Trial 2	162	75.8	1.2×10^{-13}	61.92	7864.84

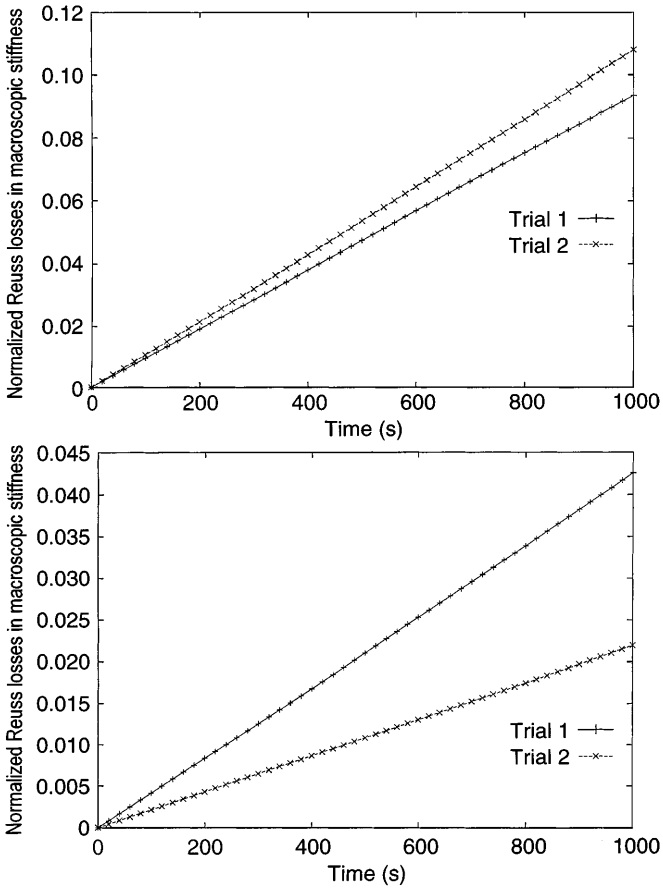

Fig. 9. Losses L_R in tension (top) and compression (bottom), with the Reuss microfield approximation at $\beta = 0.001$, $c_{crit} = 1.0$

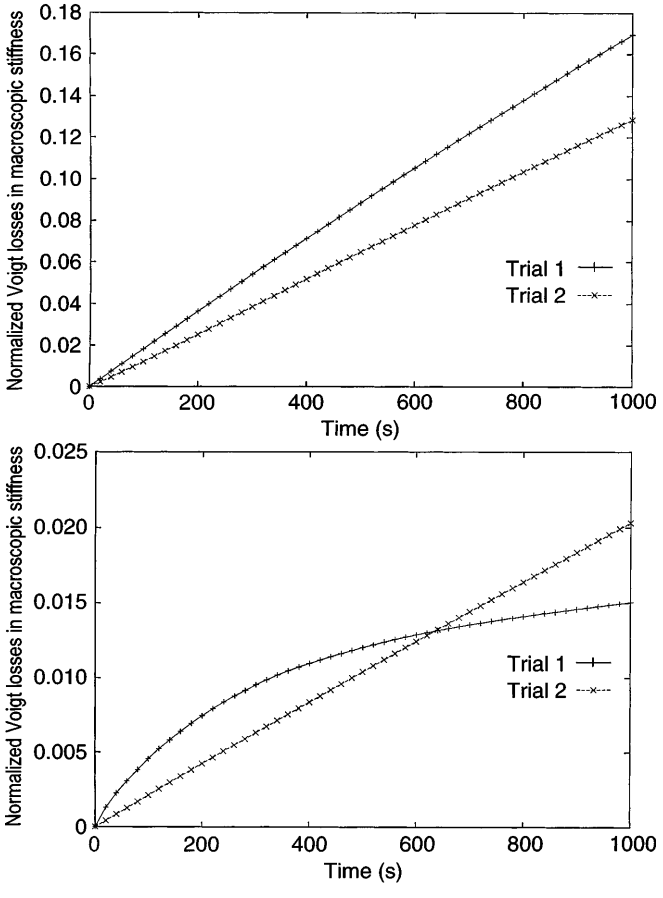

Fig. 10. Losses L_V in tension (top) and compression (bottom), with the Voigt microfield approximation at $\beta = 0.001$, $c_{crit} = 1.0$

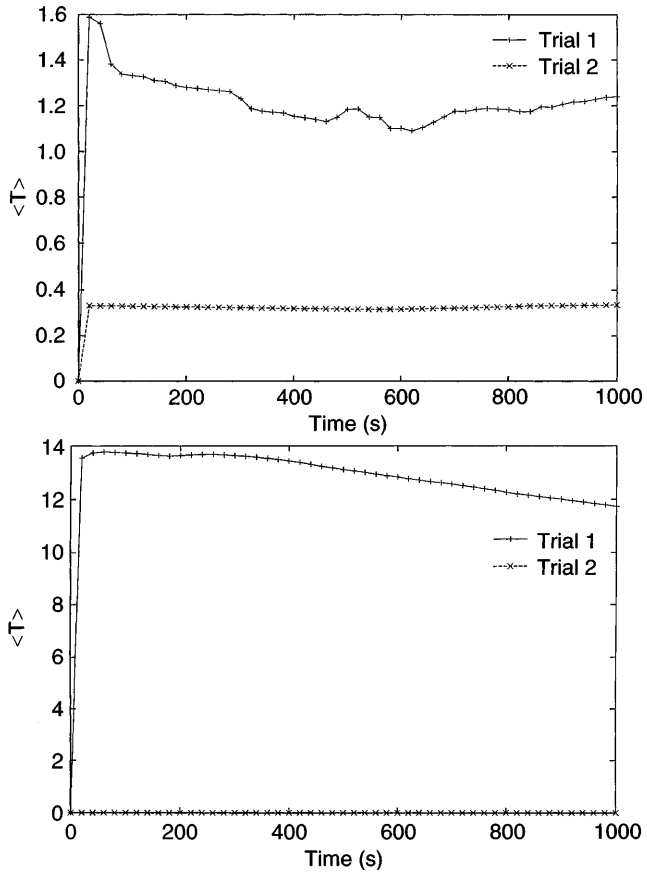

Fig. 11. The rise in average temperature in tension (top) and compression (bottom), with the Reuss microfield approximation at $\beta = 0.001$, $c_{\text{crit}} = 1.0$

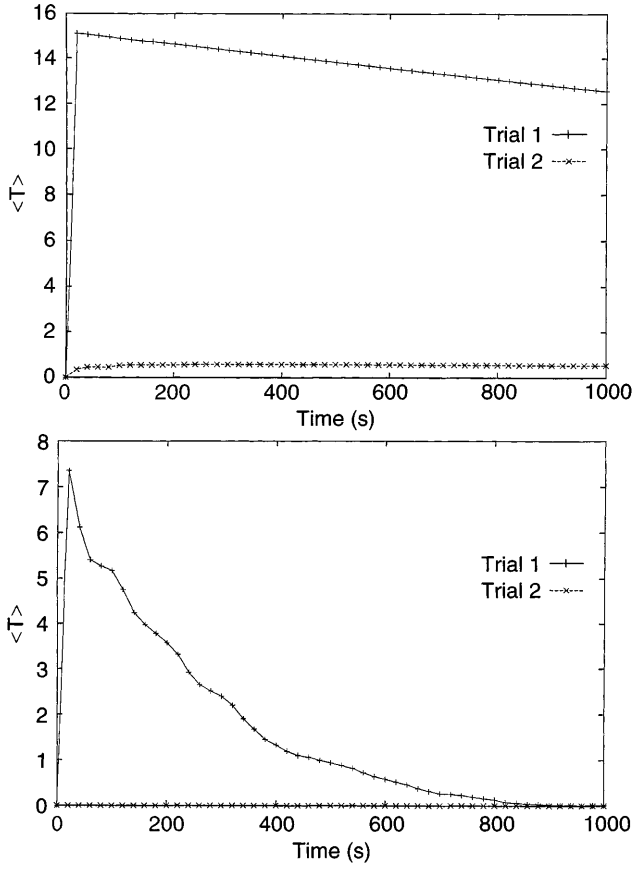

Fig. 12. The rise in average temperature in tension (top) and compression (bottom), with the Voigt microfield approximation at $\beta = 0.001$, $c_{\text{crit}} = 1.0$

References

1. **Crank, J.; Godson, S. M.:** Phil. Mag. 38 (1947) 794
2. **Crank, J.:** Phil. Mag. 39 (1948) 140
3. **Danckwerts, P. V.:** Trans. Faraday Soc. 47 (1951) 1014
4. **Odian, G.; Kruse, R. L.:** J. Polym. Sci. C22 (1969) 691
5. **Crank, J.:** The mathematics of diffusion. Oxford: Oxford Science Publications 1975
6. **Flynn, C. P.:** Point defects and diffusion. Oxford: Clarendon Press 1972
7. **Frisch, H. L.; Wang, T. T.; Kwei, T. K.:** J. Polm. Sci. A2 7 (1969) 879
8. **Wang, T. T.; Kwei, T. K.; Frisch, H. L.:** J. Polm. Sci. A2 7 (1969) 2019
9. **Van Leeuwen, H. P.:** A quantitative model of hydrogen induced grain boundary cracking. Corrosion 2 (1973) 197–204
10. **Aifantis, E. C.:** A new interpretation of diffusion in regions with high diffusivity paths: a continuum approach. Acta Metall. 27 (1979) 683–691
11. **Zohdi, T. I.; Wriggers, P.:** On the effects of microstress on macroscopic diffusion processes. Acta Mech (accepted)
12. **Zohdi, T. I.; Hutter, K.; Wriggers, P.:** A technique to describe the macroscopic pressure dependence of diffusive properties of solid materials containing heterogeneities. Computational Materials Science 15 (1999) 69–88
13. **Najar, J.:** Continuum Damage of Brittle Solids. In: Krajcinovic, D. and Lemaitre, J. (eds.) Continuum Damage Mechanics. Theory and Application pp. 231–294 Vienna/New York: Springer-Verlag 1987
14. **Troiano, A. R.:** ASM 52 (1960) 54
15. **Oriani, R. A.:** Ber. Bunse. Phyz. Chem. 76 (1972) 301
16. **Beachem, C. D.:** Metall. Trans. 3 (1972) 437
17. **Birnbaum, H. K.:** Environment-sensitive fracture of engineering materials. In: Foroulis, Z. A. (ed.) pp. 326 TMS-AIME, 1979
18. **Williams D. P.; Nelson, H. G.:** Metall. Trans. 1 (1970) 63
19. **Doig, P.; Jones, G. T.:** Metall. Trans. 8A (1977) 1977–1993
20. **Gerberich, W.W.; Livne, T.; Chen, X. F.; Kaczorowski, M.:** Crack growth from hydrogen-temperature and microstructural effects in 4340 steel. Metall. Trans. 19A (1988) 1319–1334
21. **Gerberich, W. W.; Foecke, T. J.:** Hydrogen enhanced decohesion in Fe-Si single crystal: Implications to modeling thresholds in hydrogen effects on material behavior. Moody, N. R.; Thompson, A. W. (eds.) pp. 687–702 The Minerals, Metals and Materials Society 1990
22. **Gerberich, W. W.:** Hydrogen in metals ASM Metals Park OH (1974) 115
23. **Unger, D. J.; Aifantis, D. C.:** On the theory of stress-assisted diffusion II. Acta Mech. 47 (1983) 117–151
24. **Unger, D. J.; Gerberich, W. W.; Aifantis, E. C.:** Further remarks on the implications of steady-state stress-assisted diffusion on environmental cracking. Scripta Metallurgica 16 (1982) 1059–1064
25. **Zohdi, T. I.; Meletis, E. I.:** On the intergranular hydrogen embrittlement mechanism of Al-Li alloys. Scripta Metallurgica 26 (1992) 1615–1620
26. **Zohdi, T. I.; Meletis, E. I.:** Calculation of hydrogen buildup in the neighborhood of intergranular cracks. The J. Mech. Behavior Mat. 9 No. 1 (1998) 23–33
27. **Lufrano, J.; Sofronis, P.; Birnbaum, H. K.:** Elastoplastically accomodated hydride formation and embrittlement. J. Mech. Phys. Solids 46 No. 9 (1998) 1497–1520
28. **Lufrano, J.; Sofronis, P.; Birnbaum, H. K.:** Modeling of hydrogen transport and elastically accomodated hydride formation near a crack tip. J. Mech. Phys. Solids 44 (1996) 179–205
29. **Van Der Burg, M. W. D.; Van Der Giessen, E.; Brouwer, R. C.:** Investigation of hydrogen attack in 2.25Cr-1Mo steels with a high-triaxiality void growth model. Acta Metall. 44, No. 2 (1996) 505–518
30. **Broek, D.:** Elementary engineering fracture mechanics (4th ed.) Dordrecht: Kluwer Academic Press 1991
31. **Hill, R.:** The elastic behaviour of a crystalline aggregate. Proc. Phys. Soc. A65 (1952) 349–354
32. **Hughes, T. J. R.:** The finite element method. New Jersey: Prentice-Hall 1987
33. **Ames, W.F.:** Numerical methods for partial differential equations (2nd ed.) Orlando: Academic Press 1977
34. **Axelsson, O.:** Iterative solution methods Cambridge: Cambridge University Press 1994